Monitoring ssDNA binding to the DnaB helicase from *Helicobacter pylori* by solid-state NMR spectroscopy

Thomas Wiegand, Riccardo Cadalbert, Carole Gardiennet, Joanna Timmins, Laurent Terradot, Anja Böckmann, Beat H. Meier

Monitoring ssDNA Binding to the DnaB Helicase from Helicobacter pylori by Solid-State NMR Spectroscopy

Author(s):
Wiegand, Thomas; Cadalbert, Riccardo; Gardiennet, Carole; Timmins, Joanna; Terradot, Laurent; Böckmann, Anja; Meier, Beat H.

Publication date:
2016-11-02

Permanent link:
https://doi.org/10.3929/ethz-b-000122924

Originally published in:
Angewandte Chemie. International Edition 55(45), https://doi.org/10.1002/anie.201607295

Funding acknowledgement:
159707 - NMR studies in the Solid State (SNF)

Monitoring ssDNA binding to the DnaB helicase from *Helicobacter pylori* by solid-state NMR

Thomas Wiegand[a], Riccardo Cadalbert[a], Carole Gardiennet[b,‡], Joanna Timmins[c], Laurent Terradot[b,*], Anja Böckmann[b,*] and Beat H. Meier[a,*]

[a] *Physical Chemistry, ETH Zurich, 8093 Zurich, Switzerland*

[b] *Institut de Biologie et Chimie des Protéines, Molecular Microbiology and Structural Biochemistry, UMR 5086 CNRS, Université de Lyon, 7 passage du Vercors, 69367 Lyon, France*

[c] *Université Grenoble Alpes, Institut de Biologie Structurale, F-38044 Grenoble, France ; CNRS, Institut de Biologie Structurale, F-38044 Grenoble, France and CEA, Institut de Biologie Structurale, F-38044 Grenoble, France*

[*]Corresponding authors, laurent.terradot@ibcp.fr, a.bockmann@ibcp.fr, beme@ethz.ch

‡ Present adress: *CRM2, UMR 7036 CNRS / Université de Lorraine, Faculté des Sciences et Technologies, BP 70239, Boulevard des Aiguillettes, 54506 Vandoeuvre-lès-Nancy, France*

Abstract

DnaB helicases are bacterial, ATP-driven enzymes that unwind double-stranded DNA during DNA replication. Here, we study the sequential binding of the "non-hydrolysable" ATP analogue AMP-PNP and of single-stranded (ss) DNA to the dodecameric DnaB helicase from *Helicobacter pylori* using solid-state NMR. Phosphorus cross-polarization experiments monitor the binding of AMP-PNP and DNA to the helicase. Carbon-13 chemical-shift perturbations (CSPs) are used to detect conformational changes in the protein upon binding. The helicase switches upon AMP-PNP addition into a conformation apt for ssDNA binding, and AMP-PNP is hydrolysed and released upon binding of ssDNA. Our observations shed light on the conformational changes which are triggered by the interaction with AMP-PNP and are needed for ssDNA binding of *H. pylori* DnaB *in vitro.* They also demonstrate the level of detail solid-state NMR can provide for the characterization of protein-DNA interactions and the interplay with ATP or its analogues.

The replication of genomic DNA is a central task of a cell[1] and is performed by the replisome, a multiprotein complex containing a helicase, a polymerase and a clamp loader[2]. The replisome assembles at the replication fork on DNA, where double-stranded DNA (dsDNA) is separated into single-stranded DNA (ssDNA). The unwinding of dsDNA is carried out by DnaB helicases[3] and the two resulting ssDNA strands (leading and lagging strand) serve as templates for the synthesis of daughter strands.

Bacterial DnaB helicases usually form hexameric ring assemblies[4-5], but the helicase from *Helicobacter pylori* exists as a dodecameric assembly with two stacked hexamers[6-7]. It is believed that the ring shaped helicases unwind dsDNA by a strand exclusion mechanism: one DNA strand runs through the central hole of the helicase, while the other one is excluded from it. In this process, DnaB helicases translocate along the ssDNA strands in 5' to 3' direction, using ATP as the energy source[8] and thereby generating an overwinding in the unreplicated DNA strand, which is relaxed by DNA topoisomerases[9-10]. The detailed translocation mechanism may differ from organism to organism and no complete model has been established so far.

Structurally, DnaB helicases are two-domain proteins consisting of an N-terminal domain (NTD) and a C-terminal domain (CTD). The CTD is responsible for nucleotide and ssDNA binding[11-13], as shown by biochemical studies[14] as well as X-ray crystallography[8, 13, 15-16]. Common structural features of DnaB helicases are the Walker A and B motifs that are involved in nucleotide binding and nucleotide hydrolysis[11-12]. An arginine finger of the helicase as well as a catalytic glutamate typically participate in the binding of the nucleotide to the helicase[8, 15]. The binding of a nucleotide is accompanied by the binding of a divalent metal ion, usually Mg^{2+}. Upon nucleotide addition, conformational changes have been evidenced in DnaB helicases[8, 15], but no atomistic picture is available.

We focus in this work on the structural characterisation of the interplay between the DnaB helicase from *H. pylori* (*Hp*DnaB) and the ATP-analogue Adenylyl imidophosphate (AMP-PNP) and ssDNA. All samples containing the protein were obtained by sedimentation in an ultracentrifuge[17-18], thus avoiding the difficult crystallization steps in the presence of nucleotides and/or DNA as demonstrated also in a previous NMR study on *Hp*DnaB in interaction with *Hp*DnaG[19]. The 3.2 mm rotors contained 20 mg of protein leading to a protein concentration of around 430 mg/mL.

Free AMP-PNP and AMP-PNP bound to *Hp*DnaB can be distinguished in ^{31}P NMR experiments: the free form appears in one-pulse ^{31}P NMR experiments with 10 s repetition time (where bound AMP-PNP is filtered out due to its long T_1 relaxation time) and the bound form can be observed in ^{1}H-^{31}P cross-polarization (CP) experiments[20] (which do not yield signal for free AMP-PNP, since dipolar couplings are averaged out by molecular tumbling). Figure 1a shows, for reference, a spectrum of free AMP-PNP in solution (phosphate buffer and $MgCl_2$). Figure 1b displays signals from free AMP-PNP in the solution phase of the *Hp*DnaB:$MgCl_2$:AMP-PNP sample, while Figure 1c shows the CP spectra of bound AMP-PNP confirming that the ATP-analogue is tightly bound in its initial, non-hydrolysed form to the helicase.

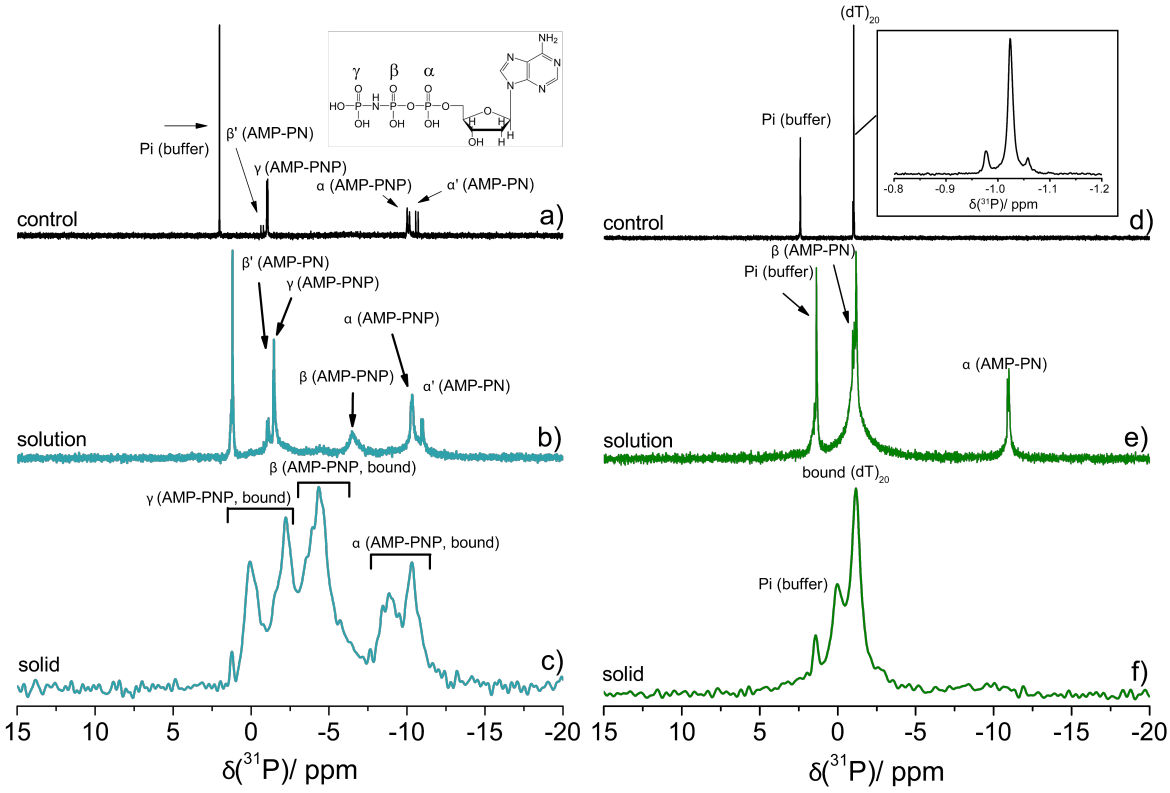

Figure 1: Binding of nucleotides and ssDNA to *Hp*DnaB: ^{31}P solution-state spectrum of a 5mM AMP-PNP and 5mM $MgCl_2$ solution in the phosphate buffer as control (a), ^{31}P solution phase (b) and ^{1}H-^{31}P CPMAS (c) spectra of the *Hp*DnaB:$MgCl_2$:AMP-PNP complex as well as a solution-state ^{31}P spectrum of a 0.5 mM $(dT)_{20}$ solution in the phosphate buffer as control (d), ^{31}P solution phase (e) and ^{1}H-^{31}P CPMAS (f) spectra of the *Hp*DnaB:$MgCl_2$:AMP-PNP:ssDNA complex. The spectrum in (b) shows a set of resonances at -1.5, -6.5 and -10.3 ppm (assigned to AMP-PNP:Mg^{2+}), as well as a less intense doublet at -1.1 and-11.0 ppm (J(^{31}P-O-^{31}P)~ 20 Hz, assigned to hydrolysed AMP-PNP, AMP-PN). The three phosphate groups of AMP-PNP can be distinguished on the basis of their chemical shifts[21]. The doublet in (a) at -10.1 ppm (J(^{31}P-O-^{31}P)~ 18 Hz) is assigned to the α-phosphate and the doublet at -1.0 ppm (J(^{31}P-N-^{31}P)~ 8 Hz) to the γ-phosphate of AMP-PNP. The numeration of phosphate groups is given on top, The β-phosphates are absent due to chemical exchange, but can be observed in the absence of Mg^{2+} (see Figure S9).

The resonances observed for *Hp*DnaB-bound AMP-PNP are slightly broadened and dispersed, indicating some conformational freedom for AMP-PNP when bound to the helicase. The ^{31}P-^{31}P 2D correlation spectrum of Figure S1 not only confirms the assignment, but also shows that there are at least three different bound AMP-PNP spin systems, probably corresponding to the two slightly different binding sites in the 3-fold symmetric hexamer and possibly being a consequence of a difference between the two hexamers constituting the dodecamer.

The conformational changes in the protein upon AMP-PNP binding are monitored in the ^{13}C DARR spectrum in Figure 2a-b and Figure S2. ^{15}N,^{13}C NCA spectra are provided in Figure S3. The ^{13}C linewidth is ~0.5 ppm for free as well as for AMP-PNP bound protein and indicates a well-ordered molecular conformation. A partial sequential resonance assignment of *Hp*DnaB was obtained on the basis of the assignment of the N-terminal domain (NTD)[22] and from 3D experiments, as described in the Supplementary Information (Figure S4)[22-23]. 25 % of the backbone atoms are assigned as detailed in Table S1.

Significant CSPs of >0.3 ppm and up to 1 ppm are detected on formation of the *Hp*DnaB:$MgCl_2$:AMP-PNP complex and are labelled in the 2D DARR spectrum presented in Figure 2 by red and orange arrows for assigned and unassigned resonances, respectively. CSP of this order of magnitude indicate local structural adaptations of the protein, but exclude major structural rearrangements (*e.g.* no sheet to helix reorientations). The residue-specific analysis of the ^{13}C CSPs was obtained using 3D spectra (Figure S5). Figure 3a summarizes the assigned CSPs, which are listed in Table S2. CSP for most residues of the NTD are below the threshold of 0.15 ppm, which we consider insignificant (and relate to experimental uncertainties), indicating the structural conservation of this domain upon AMP-PNP binding. The CTD in contrast exhibits significant CSPs (which can as a matter of fact be quantified for the assigned resonances only), many of them clustering around residues 432 to 455 (residues 437, 438, 441, 443, 448, 449, 450, 454 and 455 have CSPs > 0.3 ppm), highlighting the AMP-PNP-helicase interaction interfaces, as well as allosteric conformational changes in the helicase.

Using an 18-fold molar excess of AMP-PNP, all twelve nucleotide binding sites of a dodecamer are occupied as the resonances shift completely to their new chemical-shift positions (Figures S6 and S7). An exception is observed for residues 449A and 450T for which peak doubling (approximately 1:1, see also Figures S7 and S8) was observed with one component remaining at the original peak position. In principle, due to C3 symmetry, all resonances in a hexamer could be doubled, but for the other residues, the structural differences seem too small to be observed which is in close agreement with our findings in *Hp*DnaB[23].

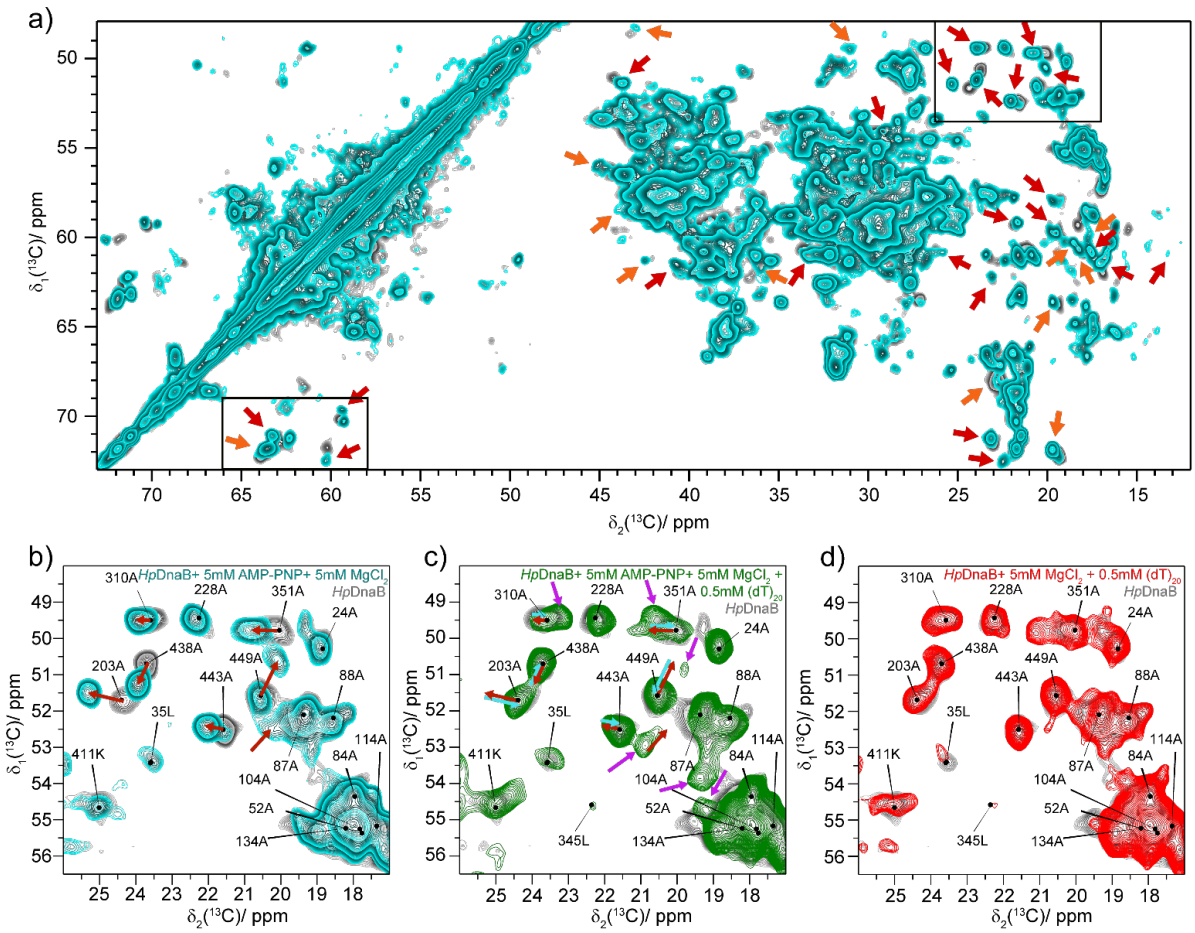

Figure 2: Chemical-shift perturbations reflect conformational changes in the helicase upon AMP-PNP binding. (a) Comparison of 20 ms ^{13}C-^{13}C DARR spectra of isolated *Hp*DnaB (grey contours) and the *Hp*DnaB:$MgCl_2$:AMP-PNP complex (cyan contours). Shifting peaks in the *Hp*DnaB:$MgCl_2$:AMP-PNP spectrum are marked by red and orange arrows for assigned and unassigned resonances, respectively. Zooms in regions shown in black frames are given in (b) for the alanine region and in Figure S2 for the threonine region. (c) Comparison of 20 ms ^{13}C-^{13}C 2D DARR spectra of *Hp*DnaB (grey contours) and *Hp*DnaB:$MgCl_2$:AMP-PNP:ssDNA (green contours). Red and cyan arrows mark shifting resonances upon AMP-PNP and upon ssDNA binding, respectively, magenta arrows indicate new appearing resonances in the spectrum of *Hp*DnaB:$MgCl_2$:AMP-PNP:ssDNA. (d) Comparison of 20 ms ^{13}C-^{13}C 2D DARR spectra of isolated *Hp*DnaB (grey contours) and *Hp*DnaB:$MgCl_2$:ssDNA (red contours). No detectable spectral changes are visible indicating only very weak binding of ssDNA to the helicase in the absence of AMP-PNP.

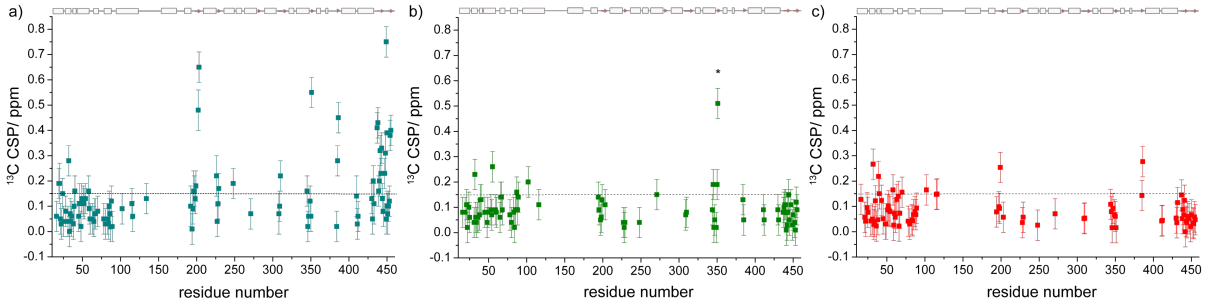

Figure 3: Site-specific ^{13}C CSPs (calculated according to $CSP = \sqrt{\frac{1}{2}\left(\Delta\delta(^{13}C^{a})^2 + \Delta\delta(^{13}C^{\beta})^2\right)}$, except for glycines for which the formula $CSP = \sqrt{\Delta\delta(^{13}C^{a})^2}$ was used) as determined from 3D experiments for (a) *Hp*DnaB:$MgCl_2$:AMP-PNP, (b) *Hp*DnaB:$MgCl_2$:AMP-PNP:ssDNA and (c) *Hp*DnaB:$MgCl_2$:ssDNA. The error bars are estimated from the differences in seven experimental spectra to be 0.06 ppm for Cα and Cβ. Secondary-structure elements as taken from the pdb files 3GXV (NTD)[24] and 4A1F (CTD)[6] are shown on top. *: Residue shows more than one resonance and the resonance with the largest CSP is given.

To characterise the DNA binding, the *Hp*DnaB:$MgCl_2$:AMP-PNP complex was reacted with ssDNA. Previous biochemical studies have shown that a 20mer of polydT binds with 3nM affinity to the helicase in the presence of AMP-PNP[7]. The ^{31}P experiments on a sample ssDNA bound to *Hp*DnaB are shown in Figures 1e-f. Technically they were performed as described above for AMP-PNP binding. The mobile solution phase spectrum of the sediment (Figure 1e) features resonances of the phosphate buffer, unbound $(dT)_{20}$, as well as AMP-PN, the hydrolysed form of AMP-PNP. The spectrum in Figure 1e was measured directly after sedimentation and shows that all AMP-PNP is hydrolysed within a few hours to AMP-PN upon ssDNA addition to the helicase (in solution without protein, AMP-PNP is still present after a week, see Figure S9). The binding of ssDNA to the protein can be seen in the ^{31}P CP spectrum of Figure 1f. The resonances between 0 and 1 ppm represent bound $(dT)_{20}$. The slight distribution of resonances may again point to a minor conformational heterogeneity of the bound ssDNA, which is not astonishing as certainly the ends of $(dT)_{20}$ are chemically different from the central nucleotides. Importantly, the spectrum shows no longer any evidence of AMP-PNP binding to the helicase, indicating that AMP-PNP is completely released in its hydrolysed form upon addition of ssDNA. The ^{31}P spectrum of *Hp*DnaB upon addition of ssDNA, but in the absence of AMP-PNP (Figure S10) shows only very weak resonances of bound ssDNA, highlighting the importance of the presence of AMP-PNP for efficient ssDNA binding.

The ^{13}C 20 ms DARR spectra[25] of the *Hp*DnaB:$MgCl_2$:AMP-PNP:ssDNA complex is shown in Figure S11 and the spectral fingerprint of the alanine region in Figure 2c (green contours) together with the spectrum of the isolated protein. As indicated by red and cyan arrows, most CSPs observed on addition of AMP-PNP are reversed upon ssDNA addition, although small spectral differences to the spectrum of isolated *Hp*DnaB persist. For the spectral region shown, a shift of 310A and 351A is observed and new weak alanine resonances are detected (all changes are marked by magenta arrows in Figure 2c). 3D NCACB spectra allow to site-specifically determine CSPs compared to the isolated protein and reveal that a majority of CSPs observed upon AMP-PNP binding (see Figure 3a) are reversed after ssDNA addition (see Figure 3b), while some new changes appear. In Figure 2d a control experiment with *Hp*DnaB reacted with $MgCl_2$ and $(dT)_{20}$ in the absence of AMP-PNP is shown confirming that AMP-PNP is indeed needed for efficient ssDNA binding (for the CSPs see Figure 3c).

Figure 4 summarizes the results from our experiments. To visualize the locus of the CSPs, a homology model based on the only available single-crystal structure of a bacterial *Hp*DnaB helicase with an ATP-analogue (the helicase from *Aquifex aeolicus* bound to ADP-Mg^{2+} [15]) was created and the determined ^{13}C CSPs were plotted on this model. Unassigned residues are given in white and grey for the two monomers. The largest CSPs (> 0.3 ppm) are found for residues located at the interface between two adjacent *Hp*DnaB monomers (see Figure 4a), both within (*e.g.* 202G, 203A, 351A, 449A) and away from the nucleotide binding site (*e.g.* 386L, 437E, 438A, 441I, 455T). Nearly all identified CSPs larger than 0.3 ppm (see Table S4) are however located in five connected strands of the eight-stranded half-beta barrel on top of which is positioned the binding site. These strands run between the nucleotide binding sites (Figure 4b) and might be slightly twisted upon insertion of the nucleotides, possibly serving as pivots that may mediate larger structural changes like ring opening/closing upon nucleotide binding.[8]

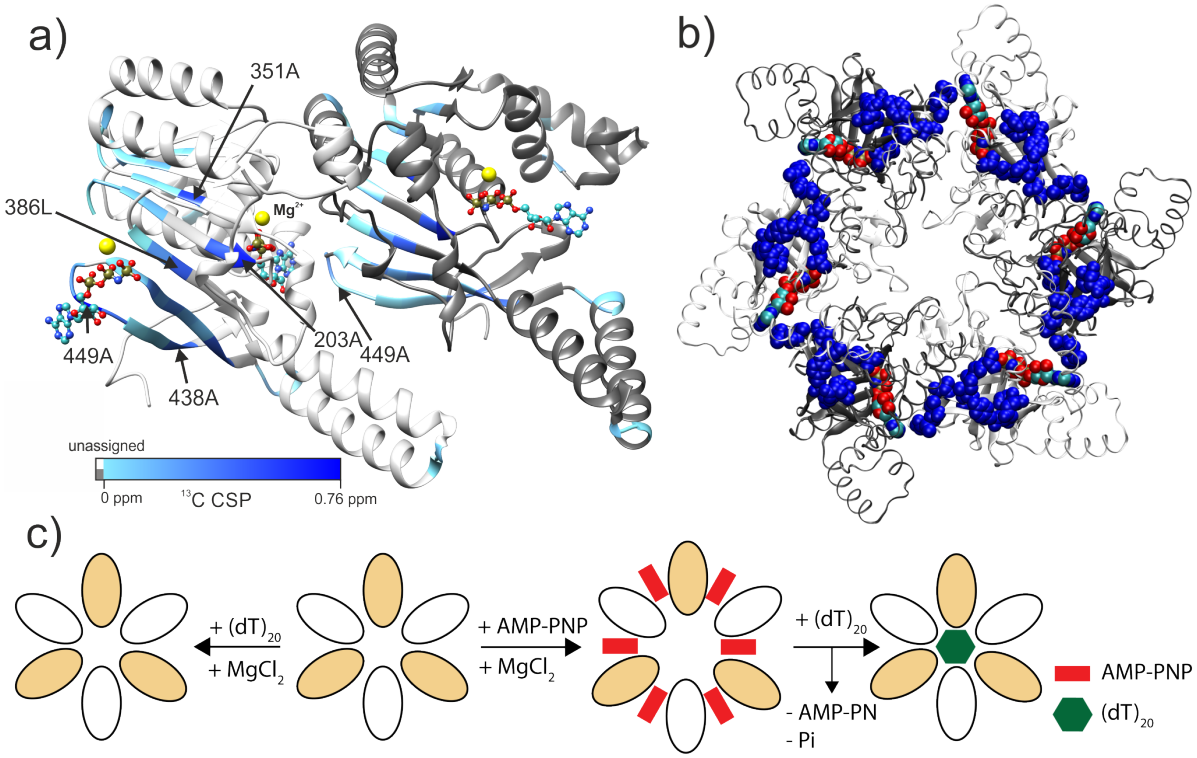

Figure 4: (a) ^{13}C CSPs plotted on a homology model based on the *Aa*DnaB:Mg^{2+}:ADP crystal structure (pdb 4NMN). Residues 195-488 of the CTD of *Hp*DnaB are shown for two monomers where unassigned residues are coloured in white and grey, respectively. ADP was replaced by AMP-PNP and is shown as CPK model and Mg^{2+} ions as yellow balls. For 449A and 450T the CSPs for the shifting resonance are shown. AMP-PNP binds in two different conformations to the helicase in agreement with the peak doubling observed for residues 449A and 450T. (b) ^{13}C CSPs > 0.3 ppm (residues shown as blue van-der-Waals balls) plotted on a complete hexamer of the homology model (residues 195 to 488 are shown). AMP-PNP is also shown as VDW balls. (c) Schematic representation of AMP-PNP and ssDNA binding to *Hp*DnaB. The *Hp*DnaB helicase is shown as hexamer as our experiments cannot distinguish hexamers from dodecamers. Upon addition of an excess of AMP-PNP and $MgCl_2$, all binding sites in the helicase are occupied, while AMP-PNP is hydrolysed and AMP-PN is released upon ssDNA addition. SsDNA in the absence of AMP-PNP binds poorly to the helicase.

We note that a crystal structure of the *Bst*DnaB:GDP:AlF_4^-:ssDNA complex is reported[8], in which only 5 out of 6 nucleotide binding sites of the helicase (which adopts a non-planar, spiral staircase conformation) are occupied by GDP molecules in the presence of ssDNA. The accessible conformational space of ssDNA:helicases thus seems rather large, and whether the observed differences are inherent to the protein, or are induced by different ATP analogues remains to be investigated.

The cartoon in Figure 4c summarizes our findings: AMP-PNP binds with high affinity at the interface between two *Hp*DnaB monomers. All AMP-PNP binding sites are occupied in the complex formed under conditions of an 18-fold molar excess of nucleotide. Two different

binding conformations (indicated by a different colouring of the ellipses representing the monomer) can be distinguished with a small, but detectable conformational freedom for AMP-PNP when bound to the helicase. The complex is competent to bind ssDNA and we could show here, that it releases AMP-PN upon binding to ssDNA, which is loaded in the central tunnel[8]. Isolated *Hp*DnaB, in the absence of AMP-PNP, interacts only weakly with ssDNA. Our data show that the presence of AMP-PNP induces a conformational switch, which might be needed to allow DNA binding to the *Hp*DnaB helicase. Upon ssDNA binding, AMP-PNP, despite its reputation as a non-hydrolysable analogue, is hydrolysed and released.

On the technical side, the study demonstrates that solid-state NMR is able to detect and follow the structural changes experienced upon chemical reactions by a complex, oligomeric motor protein from the replisome, when interacting with its "fuel" AMP-PNP and, in a second step, of the activated *Hp*DnaB:AMP-PNP complex with ssDNA. Similar experiments could find a broad application in characterizing protein-nucleotide, -DNA as well as -RNA interactions.

Acknowledgements

We thank Daniel Zindl for acquiring parts of the solution-state NMR spectra. This work was supported by the Swiss National Science Foundation (Grant 200020_159707 and 200020_146757), the French ANR (ANR-12-BS08- 0013-01, ANR-14-CE09-0024B) and the ETH Career SEED-69 16-1.

Literature

[1] J. E. Corn, J. M. Berger, *Nucleic Acids Res.* **2006**, *34*, 4082-4088.
[2] N. Y. Yao, M. O'Donnell, *Cell* **2010**, *141*, 1088-1088.e1081.
[3] J. H. LeBowitz, R. McMacken, *J. Biol. Chem.* **1986**, *261*, 4738-4748.
[4] S. Bailey, W. K. Eliason, T. A. Steitz, *Nucleic Acids Res.* **2007**, *35*, 4728-4736.
[5] S. Bailey, W. K. Eliason, T. A. Steitz, *Science* **2007**, *318*, 459-463.
[6] M. Stelter, I. Gutsche, U. Kapp, A. Bazin, G. Bajic, G. Goret, M. Jamin, J. Timmins, L. Terradot, *Structure* **2012**, *20*, 554.
[7] A. Bazin, M. V. Cherrier, I. Gutsche, J. Timmins, L. Terradot, *Nucleic Acids Res.* **2015**, *43*, 8564-8576.
[8] O. Itsathitphaisarn, Richard A. Wing, William K. Eliason, J. Wang, Thomas A. Steitz, *Cell* **2012**, *151*, 267-277.
[9] J. J. Champoux, *Annu. Rev. Biochem* **2001**, *70*, 369-413.
[10] J. C. Wang, *Nat Rev Mol Cell Biol* **2002**, *3*, 430-440.
[11] J. P. Abrahams, A. G. W. Leslie, R. Lutter, J. E. Walker, *Nature* **1994**, *370*, 621-628.
[12] J. E. Walker, M. Saraste, M. J. Runswick, N. J. Gay, *The EMBO Journal* **1982**, *1*, 945-951.
[13] E. J. Enemark, L. Joshua-Tor, *Nature* **2006**, *442*, 270-275.
[14] R. K. Soni, P. Mehra, N. R. Choudhury, G. Mukhopadhyay, S. K. Dhar, *Nucleic Acids Res.* **2003**, *31*, 6828-6840.

[15] M. S. Strycharska, E. Arias-Palomo, A. Y. Lyubimov, J. P. Erzberger, V. O'Shea, C. J. Bustamante, J. M. Berger, *Molecular cell* **2013**, *52*, 844-854.
[16] N. D. Thomsen, J. M. Berger, *Cell*, *139*, 523-534.
[17] I. Bertini, C. Luchinat, G. Parigi, E. Ravera, B. Reif, P. Turano, *Proc. Natl. Acad. Sci.* **2011**, *108*, 10396-10399.
[18] C. Gardiennet, A. K. Schütz, A. Hunkeler, B. Kunert, L. Terradot, A. Böckmann, B. H. Meier, *Angew. Chem. Int. Ed.* **2012**, *51*, 7855-7858.
[19] C. Gardiennet, T. Wiegand, A. Bazin, R. Cadalbert, B. Kunert, D. Lacabanne, I. Gutsche, L. Terradot, B. H. Meier, A. Böckmann, *J. Biomol. NMR* **2016**, *doi: 10.1007/s10858-016-0018-0.*
[20] S. R. Hartmann, E. L. Hahn, *Physical Review* **1962**, *128*, 2042-2053.
[21] S. Tran-Dinh, M. Roux, *Eur. J. Biochem.* **1977**, *76*, 245-249.
[22] T. Wiegand, C. Gardiennet, F. Ravotti, A. Bazin, B. Kunert, D. Lacabanne, R. Cadalbert, P. Güntert, L. Terradot, A. Böckmann, B. Meier, *Biomol NMR Assign* **2016**, *10*, 13-23.
[23] T. Wiegand, C. Gardiennet, R. Cadalbert, D. Lacabanne, B. Kunert, L. Terradot, A. Böckmann, B. H. Meier, *J. Biomol. NMR* **2016**, doi: 10.1007/s10858-10016-10039-10858.
[24] T. Kashav, R. Nitharwal, S. A. Abdulrehman, A. Gabdoulkhakov, W. Saenger, S. K. Dhar, S. Gourinath, *PLoS ONE* **2009**, *4*, e7515.
[25] K. Takegoshi, S. Nakamura, T. Terao, *Chem. Phys. Lett.* **2001**, *344*, 631-637.